Science of the Total Environment 664 (2019) 148–160

Contents lists available at ScienceDirect

Science of the Total Environment

journal homepage: www.elsevier.com/locate/scitotenv

A 2000-year sediment record reveals rapidly changing sedimentation and land use since the 1960s in the Upper Mara-Serengeti Ecosystem

Christopher L. Dutton [a,*], Amanda L. Subalusky [b], Troy D. Hill [c], Julie C. Aleman [a], Emma J. Rosi [b], Kennedy B. Onyango [d], Kanuni Kanuni [e], Jenny A. Cousins [f], A. Carla Staver [a], David M. Post [a]

[a] Yale University, Department of Ecology and Evolutionary Biology, 165 Prospect St, New Haven, CT 06511, USA
[b] Cary Institute of Ecosystem Studies, 2801 Sharon Turnpike, Millbrook, NY 12545, USA
[c] South Florida Natural Resources Center, National Park Service, 950 N. Krome Avenue, Homestead, FL 33030, USA
[d] WWF-Kenya, P.O. Box 62440-0020, Nairobi, Kenya
[e] WWF-Tanzania, Plot No. 350, Regent Estate Mikocheni, Dar es Salaam, Tanzania
[f] WWF-UK, The Living Planet Centre, Rufford House, Brewery Rd, Woking GU21 4LL, UK

HIGHLIGHTS

- Sediment cores from the Mara River wetland elucidate the basin's historical context.
- Most sediment comes from Upper Mara; other catchments have increased since 1960s.
- Sediment, mercury and nutrient concentrations started increasing in the 1700s.
- Large changes in the 1960s coincident with deforestation and rinderpest eradication
- The Mara Wetland is a sink for sediment and mercury coming from upstream.

GRAPHICAL ABSTRACT

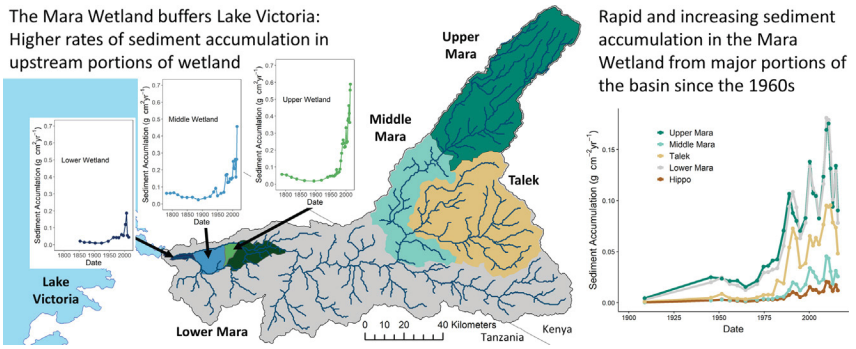

ARTICLE INFO

Article history:
Received 19 October 2018
Received in revised form 29 January 2019
Accepted 31 January 2019
Available online 01 February 2019

Editor: Filip M.G. Tack

Keywords:
Sediment core
Land use change
Deforestation
Mara River
East Africa
Lake Victoria

ABSTRACT

The Mara River basin is a trans-boundary basin of international importance. It forms the headwaters of the Nile River and serves as the primary dry season water source for an estimated 1.1 million rural people and the largest remaining overland migration of 1.4 million wildebeest in the Serengeti-Mara Ecosystem. Changes throughout the basin are impacting the quantity and quality of the Mara River, yet the historical context of environmental conditions in the basin is not well known. We collected sediment cores throughout the wetland at the mouth of the Mara River, and we used isotopic dating methods and a suite of analyses to examine historical patterns of sediment quantity and source, mercury contamination, and carbon and nutrient loading. Our results show that ecological conditions in the Mara River basin were fairly stable over paleoecological time scales (2000–1000 years before present), but there has been a period of rapid change in the basin over the last 250 years, particularly since the 1960s. A shift in the source and quantity of sediments in the river began in the late 1700s and became much more pronounced in the 1950s and 1960s, coincident with increasing mercury concentrations. The quantity of sediment from the Upper Mara increased, particularly since 1960, but the proportion of total sediment from this region decreased as the Talek and Middle Mara portions of the basin began producing more sediment. The decadal oscillation in sediment accumulation was congruent with known periods of extreme precipitation events. Carbon and nitrogen loading also increased since the 1960s, and the shift in the isotopic ratio

* Corresponding author.
E-mail address: christopher.dutton@yale.edu (C.L. Dutton).

https://doi.org/10.1016/j.scitotenv.2019.01.421

of nitrogen provides evidence for increased anthropogenic loading. Altogether, these data likely reflect patterns of change also experienced in other basins throughout East Africa.

1. Introduction

Sustainable development in Africa relies upon using natural resources to promote socioeconomic development while simultaneously protecting the ecosystem services relied upon by a large proportion of the population (McClain, 2013). Water has been identified as playing a central role in both areas (UN-Water, 2003). Water resource planning can increase human access to improved domestic water sources and improved sanitation, ensure food security through irrigated agriculture, and contribute to energy security via hydropower, while also conserving and restoring biodiversity and ecosystem services (McClain, 2013; Sharma et al., 1996; Vörösmarty et al., 2000). However, water resources are often negatively impacted by land use change associated with development patterns (Foley et al., 2005). Understanding the impacts of land use change on river basins and how they relate to historical dynamics is critically important to making informed decisions about sustainable development and to interpreting present-day patterns in quantity and quality of water resources (Kundzewicz, 1997; McClain, 2013).

The Mara River basin in East Africa is a trans-boundary river basin that highlights many of the development and conservation challenges in the region. The Mara River flows from its headwaters in the Mau Forest of Kenya through the northern portion of the Serengeti-Mara Ecosystem and into Lake Victoria in Tanzania, where it forms part of the headwaters of the Nile River basin. It is a river basin of international conservation significance, as it is the only perennial water source in the Serengeti-Mara Ecosystem, and it sustains the largest remaining overland migration of 1.4 million wildebeest that cross into this basin from the southern Serengeti during the dry season (Holdo et al., 2009). The Mara River basin also supports an estimated 1.1 million people, with over 60% of the human population directly reliant upon the river for their domestic water needs (Hoffman, 2007; LVBC and WWF-ESARPO, 2010). The basin has experienced considerable development in the past few decades, including a 27% reduction in rangelands, a 32% reduction in forest cover, and a 203% increase in agriculture between 1973 and 2003 (Mati et al., 2008).

Patterns of increasing development in the Mara River basin are similar to trends throughout East Africa. Human populations have risen steadily in Kenya and Tanzania since the 1950s (FAO, 2018). Domestic animal populations have also increased since the eradication of rinderpest in the 1960s (Raikes, 1981; Talbot and Talbot, 1963). Some wildlife populations also increased after rinderpest eradication, while multiple others began declining in the 1970s, partially due to land use changes and further increases in domestic animal populations (Ogutu et al., 2011; Ogutu et al., 2016). In the Mara River basin, these land use and land cover changes have likely altered the hydrology and water quality in the Mara River, leading to increased peak flows, increased erosion rates, and increased suspended sediments and nutrients in the river (Dutton et al., 2018; LVBC and WWF-ESARPO, 2010; Mango et al., 2011; Mati et al., 2008; McClain et al., 2014).

Increasing suspended sediment loads are a major concern in the Mara River basin; sediment loads are associated with increases in contaminant loads, and have direct potential consequences for domestic water users (Hoffman, 2007; LVBC and WWF-ESARPO, 2010). There is also widespread concern about anthropogenic contaminants in the river due to nutrient runoff from agricultural fields, human waste from urban settlements and tourism establishments, and mercury from artisanal gold mining in the basin, among other factors. Mercury contamination is a particular concern in the lower portion of the Mara River basin, because widespread artisanal gold mining commonly uses mercury in one of the processing steps (Saldarriaga-Isaza et al., 2015).

Changing populations of wildlife and domestic animals in the Mara River basin may also impact the long-term sediment and nutrient dynamics in the river. After the eradication of rinderpest, the Serengeti blue wildebeest (*Connochaetes taurinus*) herd grew from <200,000 to approximately 1.4 million by the late 1970s (Hopcraft et al., 2013), and they contribute 1100 tons of carcass biomass per year to the river through mass drownings (Subalusky et al., 2017). The Mara River also supports a large population of hippopotami (*Hippopotamus amphibius*, hippos), which has grown by 1500% from the 1950s to over 4000 individuals (Kanga et al., 2011), and they contribute 13,200 tons of biomass as feces and urine per year to the river (Subalusky et al., 2015). As wildebeest and hippo populations have recovered in the Mara, human and livestock populations also have increased (Ogutu et al., 2016).

Here, we have used sediment cores from the Mara Wetland (near its outlet into Lake Victoria) to evaluate how sedimentation rates and sources have changed historically, through a period marked by major changes in human and livestock population densities, land use, and disease epidemics (rinderpest). To do this, we evaluated sediment sources, nitrogen and carbon isotope signatures, and mercury along a transect of age-calibrated sediment cores in the Mara Wetland, from the upstream reaches to Lake Victoria. We hypothesized that sediment deposition has increased overall as human and livestock populations increased through time in the river basin. Furthermore, we hypothesized that sediment deposition would also increase as a result of land use change, including deforestation in the Upper Mara sub-catchment and increased livestock populations in the grazing lands of the Talek, Middle Mara, and Lower Mara sub-catchments, resulting in changes in sediment provenance in cores. We also hypothesized that both mercury and nutrient concentrations in the wetland would increase, and that carbon and nitrogen stable isotope ratios would shift over time to reflect changes from natural to anthropogenic sources.

2. Materials and methods

2.1. Study site

The Mara River is a trans-boundary river shared between Kenya and Tanzania (Fig. 1), and one of the more pristine basins within the greater Nile Basin of Africa (Mati et al., 2008). The Mara River basin is approximately 13,500 km^2 and ranges in elevation from 2900 m in the headwaters to 1130 m at the mouth in Lake Victoria. The Mau Forest Complex forms the headwaters of the basin and has undergone major changes since the 1970s due to legal and illegal settlements and deforestation (Olang and Kundu, 2011). The basin also hosts two conservation areas of international significance: the Maasai Mara National Reserve in Kenya and the Serengeti National Park in Tanzania.

We delineated the Mara River basin into four major sub-catchment areas (Upper Mara, Middle Mara, Lower Mara, and Talek) based upon drainage patterns from the 15 m ASTER Global DEM dataset, Version 2. The Upper Mara (2450 km^2, 18% of the basin) accounts for everything upstream of the Emarti Bridge, including the two main tributaries that form the Mara, the Nyangores and Amala rivers. This sub-catchment has small-scale settlements, small-scale agriculture and forested regions that are remnants of the largest indigenous montane forest in East Africa. The Middle Mara (3010 km^2, 22% of the basin) includes the main Mara River channel from the Emarti Bridge to the Purungat (New Mara) Bridge, which is on the border between Kenya and Tanzania. This sub-catchment primarily consists of wildlife conservancies, including portions of the Maasai Mara National Reserve, grazing

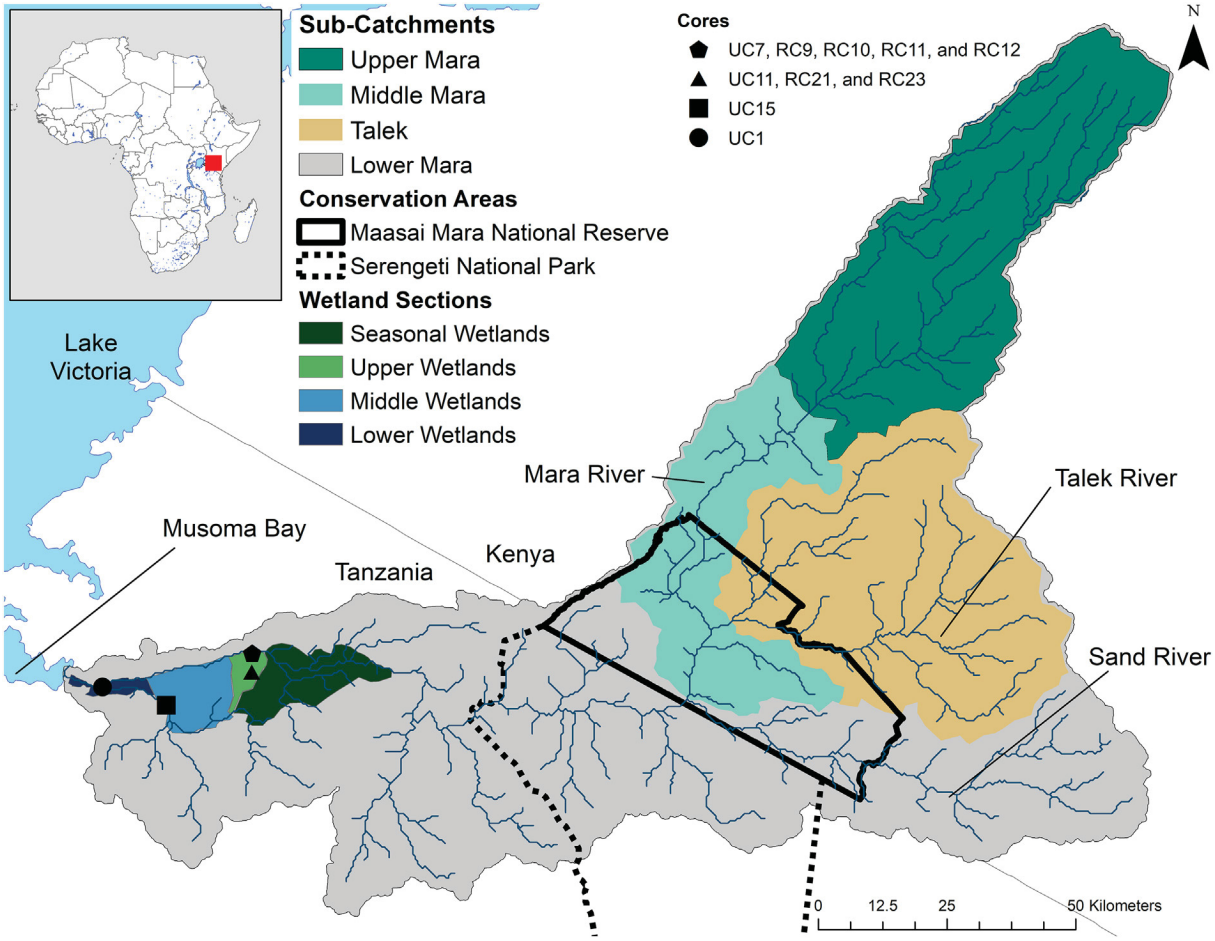

Fig. 1. The Mara River basin is a trans-boundary basin shared between Kenya and Tanzania. Sediment source fingerprints were developed for the four sub-catchments. Sediment cores were collected to represent the four sections of the Mara Wetland.

land for domestic livestock (cattle, goats, and sheep), and tourism facilities. The Lower Mara (5380 km^2, 40% of the basin) includes everything downstream of the Purungat Bridge, as well as drainage from land in Kenya near the Lamai Wedge on the west and the Sand River catchment on the east. This region includes portions of both the conservation areas of the Maasai Mara and Serengeti, and agricultural areas in Tanzania. The Talek region (2660 km^2, 20% of the basin) includes the entire catchment of the Talek River, which is a seasonal and flashy tributary draining semi-arid wildlife conservancies and grazing lands for domestic livestock. The Upper Mara receives approximately 1400 mm per year of rainfall, the Middle and Lower Mara receive approximately 1100 mm per year, and Talek receives approximately 600 mm per year (Mati et al., 2008; Mduma et al., 1999).

The Mara River flows into Lake Victoria after flowing through the Mara Wetland (also known as the Masirori swamp) near Musoma, Tanzania (Kassenga, 1997). The Mara Wetland is approximately 45 km long and up to 14 km wide. Some research suggests the Mara Wetland has expanded in size by over 300% since the 1970s, which has been hypothesized to be due to increasing sediment loads and rising lake levels (Mati et al., 2008). The Mara Wetland may play an important role in buffering the effects of land use changes in the Mara River basin on Lake Victoria (O'Sullivan et al., 2016). For example, an estimated 75 tons of nitrogen are removed yearly by the Mara Wetland (Mayo et al., 2013). Lake Victoria is the second largest freshwater body in the world and of tremendous socioeconomic importance to the region, but its ecosystem services are at risk due to deteriorating water quality, primarily caused by rivers discharging into the lake (Odada et al., 2004; Scheren et al., 2000).

We delineated the Mara Wetland into four regions (Seasonal Wetland, Upper Wetland, Middle Wetland, and Lower Wetland) based on evaluations of satellite imagery and field surveys of changes in vegetation and flow patterns conducted in August 2015. The Seasonal Wetland region is the most upstream portion of the Mara Wetland, where the river is still primarily confined to one incised channel. Small-scale agriculture takes place on the fringes of the Seasonal Wetland and, in some instances, within it. Papyrus and other common wetland plants primarily begin in the Upper Wetland section and the channel begins to bifurcate multiple times. Most of the Middle Wetland is not navigable due to dense, floating papyrus mats that impede travel. The Lower Wetland is deeper (up to 25 m) and directly tied to the hydrology of Lake Victoria. The boundaries between these regions are somewhat arbitrary and likely dynamic depending on recent precipitation. Low-impact artisanal fishing involving nets occurs within all navigable portions of the wetland.

2.2. Sediment core collection and processing

Four sets of cores were taken from the four distinct areas of the Mara Wetland. The Seasonal Wetland set of cores were taken just downstream of the Seasonal Wetland area within a constrained channel just prior to a bifurcation in the channel. The Upper Wetland core set was taken within a shallow lake (approximately 0.5 km^2) in the middle of the Upper Wetland section. The Middle Wetland core was taken in the middle portion of the wetland that was cut off from navigation from the other portions of the wetland. The Lower Wetland core was taken near the entry point into Lake Victoria (Fig. 1).

Sediments were cored from a stable, floating platform built at the site that consisted of several sheets of wood placed on two inflatable air mattresses. We collected sediment cores in August 2015, at the sediment-water interface using a Universal Corer (Aquatic Research Instruments, Hope, Idaho, USA) at four sites in distinct portions of the wetland (Fig. 1). Each Universal core (UC) included approximately 0.5 to 1 m in depth below the sediment-water interface. At two of those sites, we also collected deeper cores using a Russian Peat Borer (Aquatic Research Instruments, Hope, Idaho, USA), each segment of which was 50 cm in depth. These Russian cores (RCs) were collected at an approximately 1-meter offset from the location of the Universal cores, starting at the deepest point collected with the previous core with a 10 cm vertical overlap between each 50 cm depth intervals. Russian cores were collected to the maximum depth we were able to access by manually pushing and retrieving the corer through the wetland sediments.

Universal cores were immediately extruded and sectioned in the field into 1 cm intervals and sealed in air-tight Ziploc polyethylene bags. Entire Russian cores were sealed in the field with saran wrap to prevent desiccation and taped into PVC tubes to prevent shrinking or damage during transport. All samples were shipped wet from Tanzania to Yale University and arrived within several days.

In the lab, we processed the top core sections from all four cores (Seasonal Wetland, Upper Wetland, Middle Wetland, and Lower Wetland) for ^{210}Pb dating. We processed additional deeper cores for radiocarbon dating from the Seasonal Wetland (consisting of UC7, RC9, RC10, RC11, and RC12) and the Upper Wetland (consisting of UC11, RC21, and RC23). All Russian cores from those two sites were sectioned into 1 cm intervals. Portions of the 1 cm sections from the universal cores and Russian cores were then dried at 60 °C and re-weighed to obtain bulk mass density estimates. The dried portions were then gently disaggregated with a mortar and pestle to obtain a homogenous sample and apportioned to dating, sediment fingerprinting, carbon and nitrogen isotopic analysis, and mercury analysis.

2.3. Dating and age-depth model

We used lead-210 (^{210}Pb; 22.3 yr half-life) to assign ages to sediment deposited during the past 110 years (five half-lives). Geochemical measurements were made on subsamples dried to 60 °C. Dried, ground samples were sealed in 10 mL scintillation vials, and equilibrated for at least 21 days before analysis. This equilibration period allowed supported ^{210}Pb (^{210}Pb produced by in-situ decay of ^{226}Ra, measured indirectly as ^{214}Pb) to be distinguished from unsupported or excess ^{210}Pb ($^{210}Pb_{xs}$). Activities of ^{210}Pb and ^{214}Pb were measured by gamma ray spectrometry using a low-background Ge detector. ^{210}Pb and ^{214}Pb activities were measured at energies of 46.5 and 352.7 keV, respectively, and were corrected for detector efficiency and self-absorption (Cutshall et al., 1983).

We also measured ^{137}Cs in the upper portions of the Seasonal Wetland, Upper Wetland, Middle Wetland and Lower Wetland cores. ^{137}Cs was distributed globally during atmospheric nuclear testing in the 1950s and 1960s and can be used as an independent time marker for the age-depth model (Ritchie and McHenry, 1990).

We created age-depth models using the Plum model for the Bayesian analysis of ^{210}Pb dating for the upper portions of the Upper Wetland, Middle Wetland, and Lower Wetland cores (Aquino-López et al., 2018). We did not create an age-depth model for the Seasonal Wetland core due to mixing throughout the depth of the core (see results and discussion below). The Plum model is loosely based on the CRS model, which allows sedimentation rates to vary (Aquino-López et al., 2018; Oldfield and Appleby, 1984; Robbins, 1978). The Plum model retains two of the basic assumptions of the CRS model, including (1) that supply of ^{210}Pb is constant, and (2) that there is no vertical displacement of radionuclides (i.e., no mixing or post-depositional diagenesis). However, a continuous inventory of ^{210}Pb from the entire core is not required and it is not necessary to achieve background in order to formulate the model.

The Plum model is formulated within a robust statistical framework to natively quantify any uncertainty within the modelled dates (Aquino-López et al., 2018). Plum uses a self-adjusting Markov Chain Monte Carlo (MCMC) algorithm known as the *t*-walk (Christen and Fox, 2010). Use of the *t*-walk requires very little customization in setting the default model parameters. Changes in sedimentation accumulation are calculated through millions of iterations of the MCMC using the same gamma autoregressive semiparametric age-depth function contained within *Bacon*, a popular age-depth model for paleoclimate reconstructions (Blaauw and Christen, 2011). Full details of the Plum model formulation can be found in Aquino-López et al. (2018).

We used radiocarbon dating to date samples at longer time scales than ^{210}Pb dating. We dried samples at 45 °C and then submitted bulk sediments to the Lawrence Livermore National Laboratories (LLNL, Livermore, California, USA) for radiocarbon dating. Samples appeared homogeneous with no obvious evidence of macrofossils. All samples were subjected to the standard pretreatment steps at LLNL, including the acid-base-acid chemical pretreatment, in order to remove carbonates. Radiocarbon dating was thus performed in the total organic carbon (TOC) of the bulk sediments, preventing any potential aging effects of the carbonates (Bronk, 2008). Five radiocarbon dates were measured for the Seasonal Wetland core set (UC7, RC9, RC10, RC11, and RC12) and four radiocarbon dates were measured for the Upper Wetland core set (UC11, RC21, and RC23) (Fig. S1). The dates were calibrated using the IntCal13 curve implemented in *Bchron* in R (Parnell, 2016; Reimer et al., 2013).

We built a Bayesian age-depth model using *Bchron* in R for the Upper Wetland core (Haslett and Parnell, 2008; Parnell, 2016). In the age-depth model, we used all of the radiocarbon dates (4 total) and a subset of the ^{210}Pb-modelled dates (7 total) to prevent the age-depth model from being unfairly biased towards the ^{210}Pb-modelled dates (Fig. 4) (Kemp et al., 2013). We used the standard program settings for creation of the age-depth model (Parnell, 2016).

Sediment accretion and mass accumulation rates were calculated from $^{210}Pb_{xs}$ data for the top sections of the Upper Wetland (UC11), Middle Wetland (UC15), and Lower Wetland (UC1) cores using the Plum model for the Bayesian analysis of ^{210}Pb dating (Aquino-López et al., 2018). Sediment accretion and mass accumulation rates were also calculated for the entire Upper Wetland core set using the full age-depth model ($^{210}Pb_{xs}$ and radiocarbon dates) created in *Bchron* (Parnell, 2016). Accretion rates (r_i; cm·yr^{-1}) for each core section, *i*, at each depth, *x*, at each time, *t*, were calculated as:

$$r_i = \frac{x_i - x_{i-1}}{t_i - t_{i-1}} \quad (1)$$

Accretion rates were then used to calculate mass accumulation rates:

$$MAR_i = r_i \times \rho_i \quad (2)$$

where MAR_i is the mass accumulation rate (g·cm^{-2}·yr^{-1}) for a depth interval *i*, and ρ_i is the corresponding bulk density (g sediment·cm^{-3}).

2.4. Sediment fingerprinting

We used the sediment fingerprinting method developed in Dutton et al. (2013) to trace the source of sediments from each layer of the Seasonal Wetland and Upper Wetland cores. A brief description of our methods is described here, and a more detailed description is in Supplementary material 1.

We collected 39 composite soil samples throughout 7 different major lithology groups of the Lower Mara region to build a composite sediment fingerprint for that region (Fig. S2). Samples were dried,

gently disaggregated, and sieved to <63 μm. Samples were then analyzed for 59 elements with a multi-acid total digestion on an ICP-MS by Bureau Veritas Acme Labs (Vancouver, BC Canada).

Source signatures were previously developed for Kenyan sources (Upper Mara, Middle Mara, and Talek) and for hippos (hippo feces) for a subset of the elements analyzed during this sampling campaign (Dutton et al., 2013). We built upon those signatures by collecting additional suspended sediments from the Upper Mara ($N = 3$) and Talek ($N = 7$) from 2012 through 2015. In total, 28 elements were measured within both campaigns and considered for use as tracers. Source signatures for Upper Mara and Talek were based on suspended sediment samples collected in the river, and Middle Mara and Lower Mara were based on soil samples from the different lithologies of those subcatchments. We minimized potential artifacts of these different sample types by only analyzing the fine fraction of the soil samples (<0.63 μm), which is a widely accepted approach to reduce potential particle size influence on elemental signatures (Collins et al., 2017). Additionally, we collected suspended sediment samples during different flow events and discharges to capture the natural variability occurring within each sub-catchment (Dutton et al., 2013).

We used a simplified tracer screening approach similar to Blake et al. (2018). First, we removed elemental concentrations from the depositional samples that fell outside the minimum detection limits or the natural range of the sources. We then used a Kruskal-Wallis *H*-test to identify tracers that showed significant differences between the potential sources (Supplementary material 2) (Kruskal and Wallis, 1952; R Core Team, 2018). To characterize the discrimination ability of the combination of elements, we used a step-wise Discriminant Function Analysis (DFA) based on the minimization of Wilk's lambda and a jackknifed Discriminant Function Analysis (jDFA) (Venables and Ripley, 2002; Weihs et al., 2005). Overall success with the leave-one-out classification (jDFA) was 93%. We then used MixSIAR, a Bayesian mixing model, to estimate the source proportions for each core slice (Moore and Semmens, 2008; Stock et al., 2018; Stock and Semmens, 2016). We then applied the Bayesian age-depth model incorporating the modelled ^{210}Pb and radiocarbon dates to the source proportions for each core slice to determine sediment source proportions through time.

2.5. Mercury

We measured total mercury concentration in sediment layers from universal cores from three different locations along a transect through the Mara Wetland: Upper Wetland, Middle Wetland and Lower Wetland (Fig. 1). Samples were dried, ground with a mortar and pestle, and analyzed on a Direct Mercury Analyzer (DMA80, Milestone, Shelton, CT, USA).

2.6. Carbon and nitrogen isotopes

The dried and ground sediment samples from the Upper Wetland core set (UC11, RC21, and RC23) were fumigated in hydrochloric acid vapor for 48 h to remove inorganic C (Jaschinski et al., 2008; Ramnarine et al., 2011). We then measured the percent by mass of total organic carbon and total nitrogen, as well as the stable isotope ratios of carbon (total organic $\delta^{13}C$) and nitrogen (total $\delta^{15}N$), on a Costech elemental analyzer (Costech Analytical Technologies Inc., Valencia, CA, USA). Stable isotope ratios were normalized to air ($\delta^{15}N$) and Vienna Pee Dee Belemnite ($\delta^{13}C$) scales and reported in per mil notation, where $\delta^{15}N = [(R_{sample} - R_{air}) / R_{air}] \times 10^3$ and $\delta^{13}C = [(R_{sample} - R_{PDB}) / R_{PDB}] \times 10^3$.

All statistical analyses were computed in R 3.5.1 in RStudio 1.1.453 (R Core Team, 2018; RStudio Team, 2016). All R code and data for conducting the analyses and preparing the figures are provided in Supplementary materials 1, 2, 3, and the Mendeley Data online data repository (Dutton et al., 2019).

3. Results

3.1. Dating and age-depth model

The Seasonal Wetland core showed evidence of mixing throughout the upper portion of the core with no discernable pattern in the ^{210}Pb data (Fig. 2). The radiocarbon dating chronology for the Seasonal Wetland core set (UC7, RC9, RC10, RC11, and RC12) further indicated a strong mixing of sediments (Table 1). We found ^{14}C ages alternating between modern and approximately 300 [yr BP] from 4 tested samples down to at least 159 cm below the sediment surface (Table 1). The bottom of the deepest part of that core set (RC12) was at 189 cm below the sediment surface and it was dated at 2625 ± 50 ^{14}C age [yr BP] (Table 1), indicating that the mixing zone within that core set stopped somewhere between 159 cm and 189 cm. Mixing of sediments within this core was likely due to the geomorphology of this wetland section and the presence of frequent disturbances in the channel. The river flows through a constrained channel at this sampling point, and we sampled immediately upstream of a bifurcation in the channel where we believed sediment would accumulate. However, the data suggest this location was not a stable depositional zone, so we did not create an age-depth model for this core.

Excess ^{210}Pb activity from the Upper Wetland, Middle Wetland, and Lower Wetland showed a general decrease in activity through the depth of the core and the potential presence of mixing in the upper portion of the cores. Bayesian-modelled dates based on the excess ^{210}Pb activity were computed for each depth in the Upper Wetland, Middle Wetland and Lower Wetland cores (Figs. 2 and 3). In all three cores, the Plum age-depth model indicated more rapid sediment accretion and accumulation in recent years; however, this pattern was more pronounced in the Upper Wetland core and declined going downstream to Lake Victoria (Upper Wetland, Middle Wetland, and Lower Wetland) (Fig. 4). Model confidence was greatest in the Upper Wetland core (Fig. 3).

The use of ^{210}Pb derived age-depth models requires an independent corroboration to establish that the model is reasonable (Smith, 2001). We attempted to use ^{137}Cs as an independent time marker but detected very low levels of it in all four cores (Fig. S3). The Upper Wetland Core had a small peak at 29 cm that doubled background levels (~6 Bq kg^{-1}). We constructed an age-depth model for the Upper Wetland core using the ^{210}Pb data and the independent time marker of the ^{137}Cs peak and the dates after 1960 were very similar. However, accumulation rates and dates prior to 1960 were non-sensical (indicating an exponential decrease in erosion between the 1950s and 1960s, see Supplementary material 2), so we utilized the age-depth model without the use of the ^{137}Cs peak. Our inability to utilize ^{137}Cs in this system may be due to the general low levels of fallout in the southern hemisphere and because ^{137}Cs may be non-conservative and mobile in the anoxic sediments of the Mara Wetland (Benoit and Rozan, 2001; Comans et al., 1989; Davis et al., 1984; Drexler et al., 2018; Wang et al., 2017). Other studies in equatorial Africa have also reported low ^{137}Cs levels that made the radioisotope unreliable as an independent stratigraphic marker (Nyarko et al., 2016). Because we were unable to use ^{137}Cs as an independent time marker, we compared our age-depth models to historical trends of precipitation, the historical water level of Lake Victoria, and prior watershed erosion modelling to establish that our ^{210}Pb derived age-depth models are reasonable (see discussion).

Elevated ^{210}Pb concentrations in the Upper Wetland core suggest that ^{210}Pb has been imported to this area in excess of expected atmospheric deposition (Turekian et al., 1983). It is likely that land use changes within the basin and variable inputs of rainfall and sedimentation since the 1960s affected the ^{210}Pb input to the wetland (Baskaran et al., 2014). Although the concentrations diverge substantially, the modelled sediment accumulation rates are quite similar overall (Fig. 4), providing some confidence that artifacts are temporally

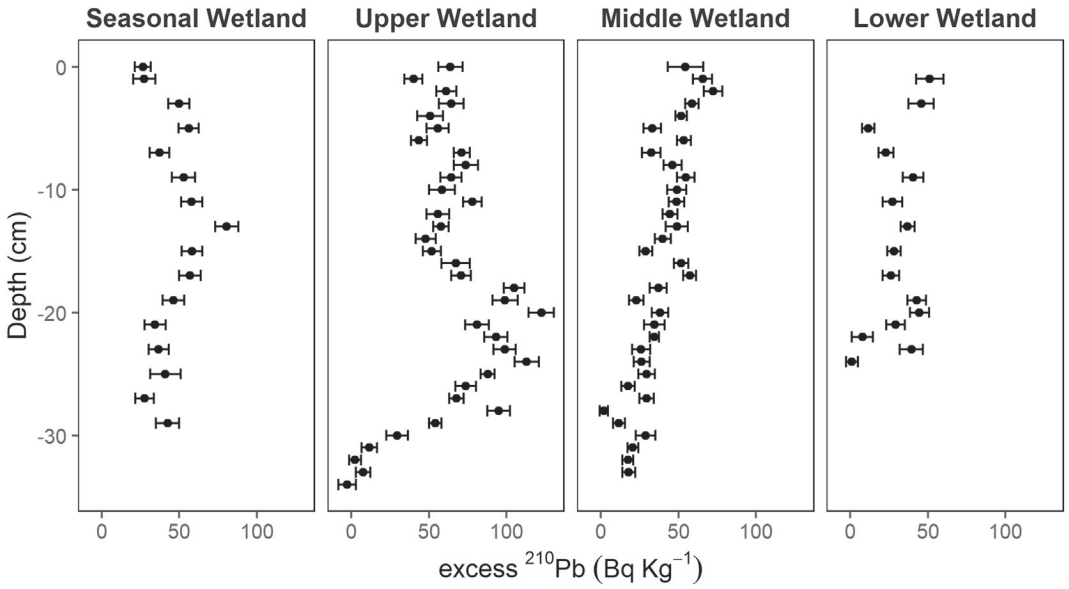

Fig. 2. Excess ^{210}Pb concentrations (mean and standard deviation) for the four cores (Seasonal Wetland, Upper Wetland, Middle Wetland, and Lower Wetland).

constant or otherwise insubstantial and accounted for within the confidence intervals of the Plum Bayesian model.

The radiocarbon dating chronology for the Upper Wetland core set (UC11, RC21, and RC23) showed that the core ranged from present to 1839 years BP (Table 1). Results from the Bayesian age-depth model indicated that sediment deposition was not linear through time, and that deposition rates were most rapid in recent years (Fig. 5).

3.2. Sediment fingerprinting

We found changing sediment sources over time in the Upper Wetland Core set (UC11, RC21, and RC23) (Fig. 6). The Upper Mara was responsible for the greatest proportion of sediments throughout the set of Upper Wetland cores (Fig. 6). Lower Mara and Talek sources make up the next two largest sources of sediment in the core. The proportion of sediments from Upper Mara began declining in the late 1700s, with the other sources increasing in proportion. Changes became most pronounced in the mid-1970s (Fig. 6). The proportion of sediment contributed by the Upper Mara declined markedly from ~50–60% of the sediments in the wetland to ~40% in the late 1980s. At the same time, sediment contribution from the Talek portion of the basin increased from <10% to ~20%. Sediment loads from the Lower Mara have provided approximately the same proportion of sediments relative to the other sources (~30%).

In addition to changes in the source of sediments, the total amount of sediment accumulating in the wetland from each portion of the basin has continued to increase, particularly since the 1960s, coincident with the rise in populations of human and cattle in Kenya and Tanzania (Fig. 7A and B). The largest quantity of sediment is provided by the Upper Mara, followed by Lower Mara and then Talek and Middle Mara.

The MixSIAR mixing model confirmed that the core slices in the Seasonal Wetland core (UC7) are all likely well mixed with one another, with no change in sediment source over the depth of the core (Fig. S4). Plots of key elements as well as bulk density, nitrogen, carbon, and mercury, confirm a relatively homogeneous upper core section indicative of a mixed column of sediments (Figs. S5 and S6). In contrast, plots of key elements from the non-mixed Upper Wetland core exhibited clear changing patterns throughout the depth of the core in multiple elements (Figs. S7 and S8) which would be indicative of a non-mixed core.

Table 1
Radiocarbon chronology of the Seasonal Wetland core set (UC7, RC9, RC10, RC11, and RC12) and the Upper Wetland core set (UC11, RC21, RC23) from the Mara Wetland.

Laboratory code	Material	Core set	Core	Depth (cm)	Thickness (cm)	14C age [yr BP]	Calibrated age [cal yr BP, ±1 σ][a]
CAMS# 173870	TOC of bulk sediment	Seasonal wetland	RC9	48	1	300 ± 30	362 ± 106
CAMS# 173869	TOC of bulk sediment	Seasonal wetland	RC10	88	1	Modern	Modern
CAMS# 173871	TOC of bulk sediment	Seasonal wetland	RC11	128	1	285 ± 30	336 ± 119
CAMS# 174604	TOC of bulk sediment	Seasonal wetland	RC12	159	1	Modern	Modern
CAMS# 172566	TOC of bulk sediment	Seasonal wetland	RC12	189	1	2625 ± 50	2691 ± 147
CAMS# 174605	TOC of bulk sediment	Upper wetland	UC11	44	1	995 ± 45	898 ± 97
CAMS# 174606	TOC of bulk sediment	Upper wetland	RC21	67	1	1445 ± 35	1393 ± 74
CAMS# 174607	TOC of bulk sediment	Upper wetland	RC23	97	1	1610 ± 40	1518 ± 102
CAMS# 172565	TOC of bulk sediment	Upper wetland	RC23	124	1	1910 ± 45	1839 ± 119

[a] Using the IntCal13 calibration curve (Reimer et al., 2013) in *Bchron* in R (Parnell, 2016).

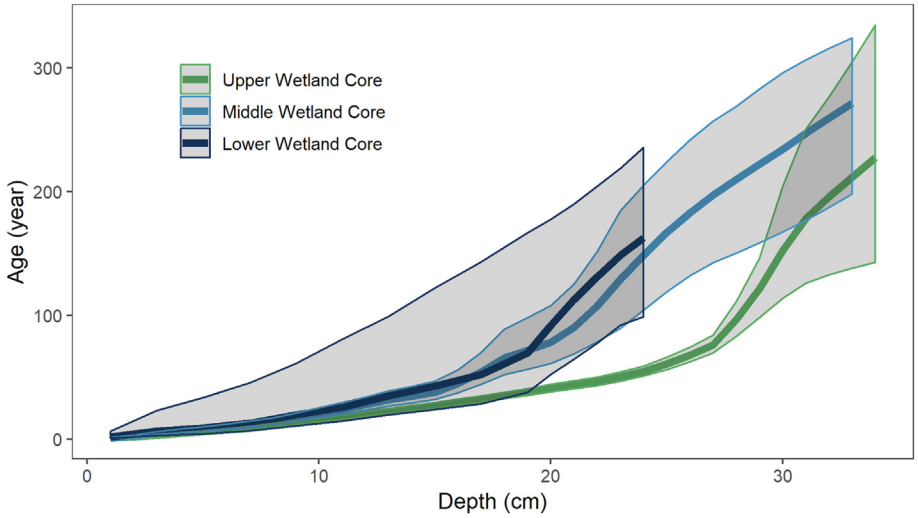

Fig. 3. Plum Bayesian age-depth models for the Upper Wetland core (light green), Middle Wetland core (light blue) and Lower Wetland core (dark blue). Shaded area represents 95% confidence region. Colors match the wetland regions represented in Fig. 1.

3.3. Mercury

Mercury data for the Upper Wetland core had a historic baseline ~20 ppb that began increasing gradually in the 1700s (Fig. 8A). Concentrations briefly stabilized at ~30 ppb in the 1950s before increasing in the 1960s to ~50 ppb, which is 2.5 times historic background concentrations. In 1984, concentrations began declining to ~25 ppb, found in the upper region of this core.

We also examined patterns in mercury concentration over the last 50–100 years along a transect through the wetland (Fig. 8B). Mercury concentrations in the Middle Wetland core increased from 25 to 35 ppb from 1950 to 2000, which is similar to the concentration changes in the Upper Wetland core. Concentrations have begun to increase again at this site in the last 20 years, rather than declining as at the Upper Wetland site. The Lower Wetland core shows a different pattern, with a slight decrease in mercury levels from 1900 to 1990, followed by a sharp decrease and recovery of mercury concentrations (Fig. 8B).

3.4. Carbon and nitrogen isotopes

The percent C and N in the Upper Wetland began increasing in the early 1900s, peaked from 1960 to 80, and then declined to levels just below the historic baseline from 1990 to present (Fig. 9A). Interestingly, both the percent C and N, and the C:N ratio (Fig. S9), declined through the 1970s and 80s to modern-day levels.

C and N stable isotope ratios follow different patterns over this time period (Fig. 9B). Looking at a longer historical time period, from 1000 to 1950 CE, $\delta^{13}C$ is relatively constant at −14 to −16‰, which aligns with the isotopic ratio of C4 savanna grasses in the Mara watershed (Fig. 9B) (Masese et al., 2015; Masese et al., 2018). From ~1950–70, this value declines to −20‰, which is closer to the ratio of C3 plants such as trees. The $\delta^{13}C$ ratio then increases in 1980–90 to an intermediate value of −17‰.

For $\delta^{15}N$ ratios, the historical baseline was relatively stable between 2 and 4‰ from 1000 to 1960 (Fig. 9B). The $\delta^{15}N$ ratio increased gradually from 1960 to 1980, and then increased dramatically through the 1990s, when it stabilized at elevated values around 6‰ over the past 20 years.

4. Discussion

Multiple lines of evidence suggest ecological conditions in the Mara River basin were fairly stable over paleoecological time scales (2000–1000 years before present), but there has been a period of rapid change in the basin over the last 250 years, particularly since the

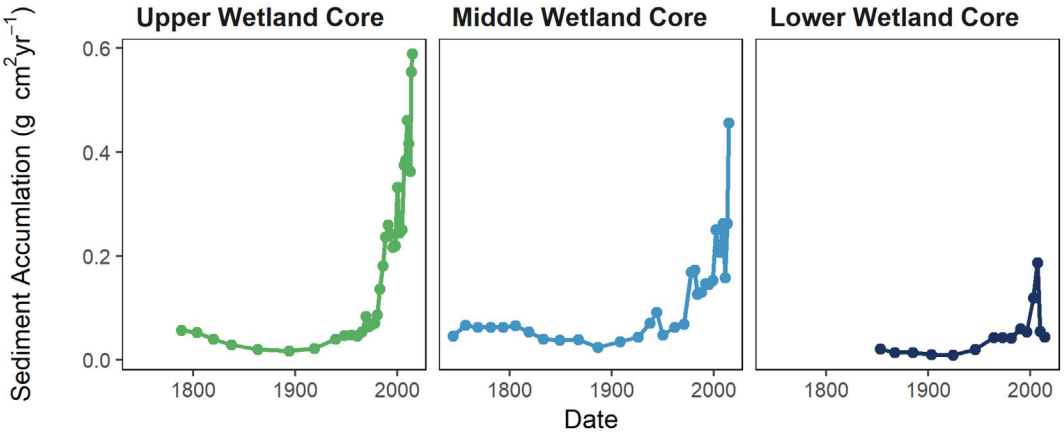

Fig. 4. Sediment accumulation chronologies in cores from a lake in the Upper Wetland (UC11, left column), the Middle Wetland (UC15, middle column) and the Lower Wetland near Lake Victoria (UC1, right column) using the Plum model. Colors match the wetland regions represented in Fig. 1.

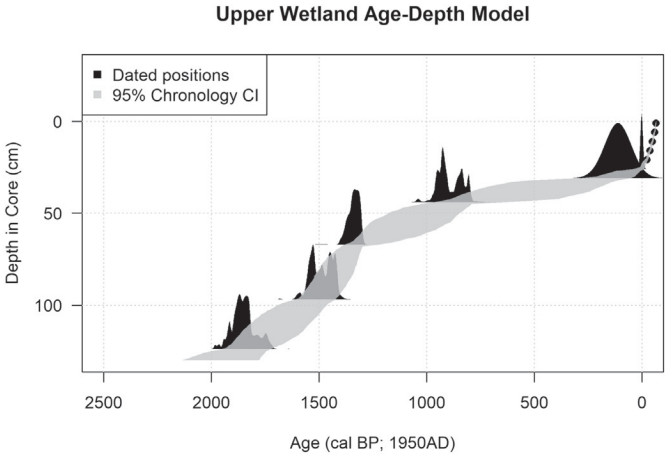

Fig. 5. Bayesian age-depth model for the Upper Wetland core set (UC11, RC21, and RC23) using radiocarbon and ^{210}Pb dating. Points and the two density probability curves on the right represent the ^{210}Pb dates from the Plum Bayesian age-depth model (taken every 5 cm, 7 dates total); radiocarbon dates are represented as the four density of probability curves on the left (Parnell, 2016). Age in 'cal BP' refers to the age in calibrated years before present, the present being 1950 by convention.

1960s, likely due to anthropogenic factors. The earliest changes in the basin began in the mid-1700s, including increased sediment, mercury, and nutrient loads, and these changes corresponded with the advent of the Industrial Revolution and the increased presence of colonial settlers in East Africa by the late 1800s (Shillington, 2012). More pronounced changes in the origin and quantity of sediments, mercury concentrations, and C and N stable isotope ratios began in the 1960s.

The highest proportion of suspended sediment has always come from the Upper Mara, which is to be expected since this region has the highest elevational changes and the highest rainfall (McClain et al., 2014). However, the proportion of total sediment entering the wetland from the Upper Mara region has decreased from ~50% to ~40% since the late 1700s, and particularly in the 1950s and 1960s, even as the quantity of sediment from the Upper Mara has increased (Figs. 6 and 7). Much of this change in proportional load is due to increased quantity and proportion of sediment from the Talek portion of the basin, which increased from <10% of total sediments in the 1970s to ~20% in recent years.

Contemporary research from 2011 through 2014 measuring high temporal resolution sediment fluxes found that the combined Middle Mara-Talek sub-catchment contributes twice the sediment flux as the Upper Mara sub-catchment (Dutton et al., 2018). This study found that the Middle Mara and Talek sub-catchments contributed an average of 8% and 21% of the sediments from 2010 through 2015 compared to 33% from the Upper Mara. Although within the same order of magnitude, the difference between the two methods may reflect the transport and storage of sediments within the river channel or banks. Sediments mobilized from Talek and other areas of the basin may take several years to decades to reach the wetland. Previous studies have shown the floodplains and river channels are important for sediment storage dynamics in rivers (Wallbrink et al., 1998; Walling et al., 2003). Overall, these data suggest recent land-use change in the Talek may be causing this portion of the basin to become an increasingly important source of sediments in the region which have not yet reached the wetland. A delay in the timing between when sediment is mobilized in the catchment and when it reaches the Mara Wetland would suggest there may be some error in our estimates of the time of land use change in the basin. However, we expect this time lag to be relatively short, given the alignment of sediment dynamics in the wetland with known timing of land use change in the basin.

Our findings provide support for earlier work using remote sensing showing that the Mara Wetland has expanded in size since the 1970s due to sediment accumulation in the upper portions of the wetland (Mati et al., 2008). In all the cores analyzed, the Plum Bayesian age-depth models indicate more rapid sediment accumulation in recent decades (Fig. 4). As sediment deposition accelerated, the Plum models suggest the wetland served as a sediment trap, with higher rates of sediment accumulation occurring in the upstream portions away from Lake Victoria. Interestingly, the age-depth model indicated that sediment accumulation rose rapidly in the Lower Wetland after 1996 and fell again just prior to 2009 (Fig. 4). This change likely coincided with a rapid increase in the water level of Lake Victoria in 1998 and subsequent decline in water level up to 2007 (Vanderkelen et al., 2018). As Lake Victoria rose, hydrological connectivity likely increased between the lower and middle portions of the wetland and the mainstem river upstream, which would have reduced water residence time in the wetland and the corresponding buffering capacity of wetland vegetation and allowed more sedimentation to reach further through the wetland towards Lake Victoria (Bavor and Waters, 2008; Kansiime et al., 2007). A similar, but smaller, peak was also observed in the Middle Wetland between 1998 and 2009 (Fig. 4).

Sediment accumulation dynamics in the wetland also likely reflect large-scale precipitation patterns in the basin. The sediment fingerprinting analysis from the Upper Wetland core identified an overall increase in sediment accumulation from all sources since the 1960s. However, there has been an oscillation in sediment accumulation

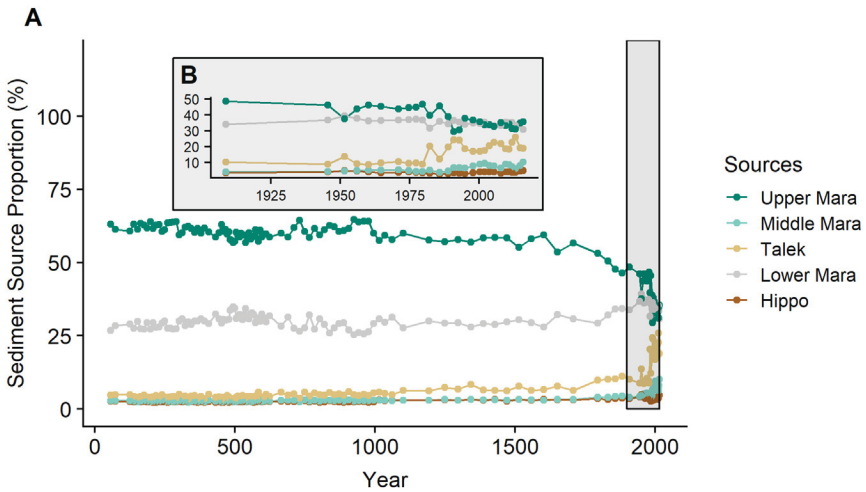

Fig. 6. A. Sediment fingerprinting source proportion in the Upper Wetland set of cores (UC11, RC21, RC23) for approximately 2000 years. Source proportions from 1900 to present day highlighted in gray. B. Source proportions from 1900 to present day. Colors match the regions represented in Fig. 1.

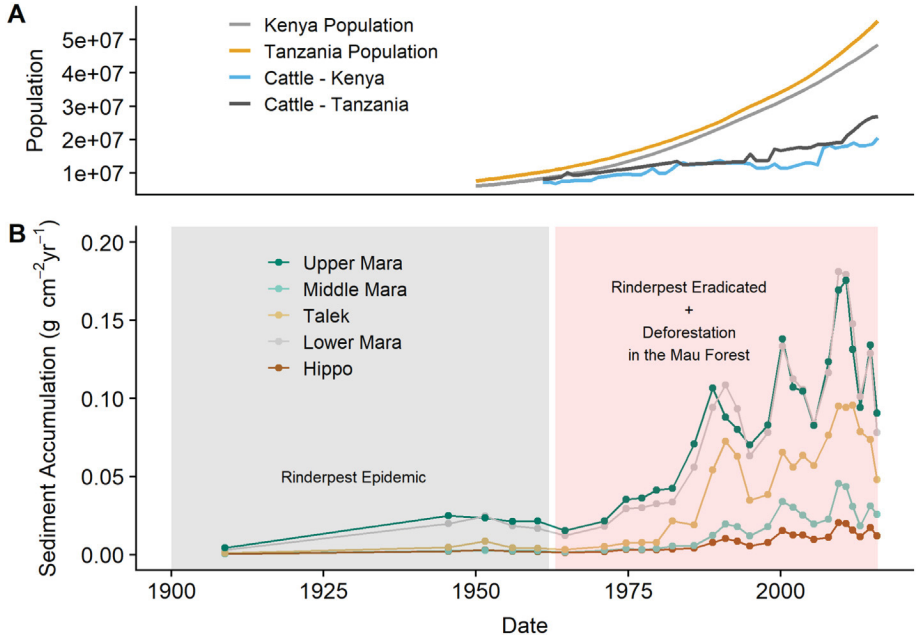

Fig. 7. A. Kenya and Tanzania human population and cattle population numbers from 1950 to present (FAO, 2018). B. Sediment accumulation from 1900 to present day in the Upper Wetland Core (UC11). Colors match the regions represented in Fig. 1. Gray box indicates the time of the rinderpest epidemic in the Mara-Serengeti (~1894–1962) (Talbot and Talbot, 1963). Red box indicates the eradication of Rinderpest in the Mara-Serengeti and the deforestation in the Mau Forest (~1964–Present) (Baldyga et al., 2008; Talbot and Talbot, 1963).

rates from all sources since the late 1970s (Fig. 7B). This pattern may reflect the natural decadal oscillation in rainfall patterns in concert with increasing rainfall extremes experienced in the Mara since the 1960s (Fig. 10) (Bartzke et al., 2018). A series of wetter years with extreme floods would be capable of transporting more sediments than those transported by the succeeding period of drier years with extreme droughts. The sediment accumulation rates from the age-depth model roughly corresponded to historical rainfall records, showing decreased sediment accumulation rates in periods of extreme droughts and higher sediment accumulation rates after periods of higher annual rainfall (Fig. 10).

Further support for our age-depth models and sediment accumulation rates can be found by comparing our sediment accumulation rates to modelled erosion rates using land use, slope, and soil characteristics in the basin. Using land cover data from 2003, Defersha et al. (2012) used the *Erosion 3D* model to calculate the expected amount of erosion in the combined Upper Mara, Middle Mara and Talek sub-catchments to be 0.3 g cm^{-2} yr^{-1}. Using the results of our age-depth model, sediment fingerprinting proportions and calculated sediment accumulation rates, we found that the amount of erosion in 2003 from the combined Upper Mara, Middle Mara and Talek sub-catchments was approximately 0.2 g cm^{-2} yr^{-1} (95% confidence intervals between 0.08 and 0.35 g cm^{-2} yr^{-1}, Fig. 7). Additionally, the trend of a contemporary increase in sediment accumulation rate found with our ^{210}Pb age-depth model is independently supported by an increase in modelled erosion rates based on satellite-derived land cover changes using the Revised Universal Soil Loss Equation in the Lower Mara sub-catchment between 1986 and 2013 (Århem and Fredén, 2014), and satellite-derived land cover changes from the Upper Mara, Middle Mara, and Talek sub-catchments between 1976 and 2014 indicating an increase in agricultural lands (Mwangi et al., 2018), which historically accounts for the highest rate of erosion in the basin (Defersha et al., 2012). Contemporary high temporal resolution measurements from 2012 to 2015 of suspended sediment flux from the Upper Mara, Middle Mara and Talek sub-catchments also indicate the potential for yearly increases, although yearly trends were not calculated because several months were missing from each hydrological year (Dutton et al., 2018).

Age-depth modelling using ^{210}Pb in catchments with dynamic sediment regimes can be challenging (Abril et al., 2018; Kirchner, 2011). Data that violates the age-depth model assumptions can lead to incorrect dates and spurious sediment accumulation rates (Abril et al., 2018; Bachmann et al., 2018). The Plum model we use to analyze ^{210}Pb dating is based on the CRS model, but does not require that ^{210}Pb measurements quantify the total inventory of ^{210}Pb (Aquino-López et al., 2018; Mabit et al., 2014). The non-monotonic decreases in ^{210}Pb that we observed in the upper portion of our cores could represent an increase in the sediment accumulation rate or the presence of mixing (Arias-Ortiz et al., 2018), which can result in an overestimation of sediment accumulation rates (Arias-Ortiz et al., 2018; Mabit et al., 2014). Our ^{210}Pb concentrations by depth may not represent the ideal conditions for age-depth modelling, so we have used both independent corroborations of our estimated sedimentation rate and a statistical framework that incorporates uncertainty (Aquino-López et al., 2018). Additionally, we focus our analysis on decadal trends in the upper

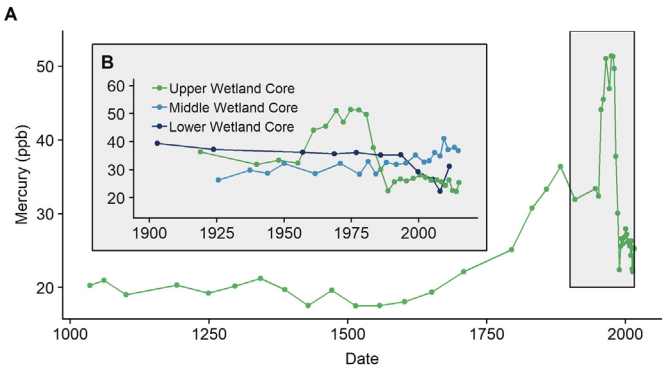

Fig. 8. A. Mercury concentration (in parts per billion) in a sediment core from the Upper Wetland from 1100 CE to present day. Mercury concentrations from 1900 to the present day highlighted in the gray box. B. Mercury concentrations (in parts per billion) from the Upper Wetland (red), Middle Wetland (orange) and Lower Wetland (blue) sediment cores. Colors match the regions represented in Fig. 1.

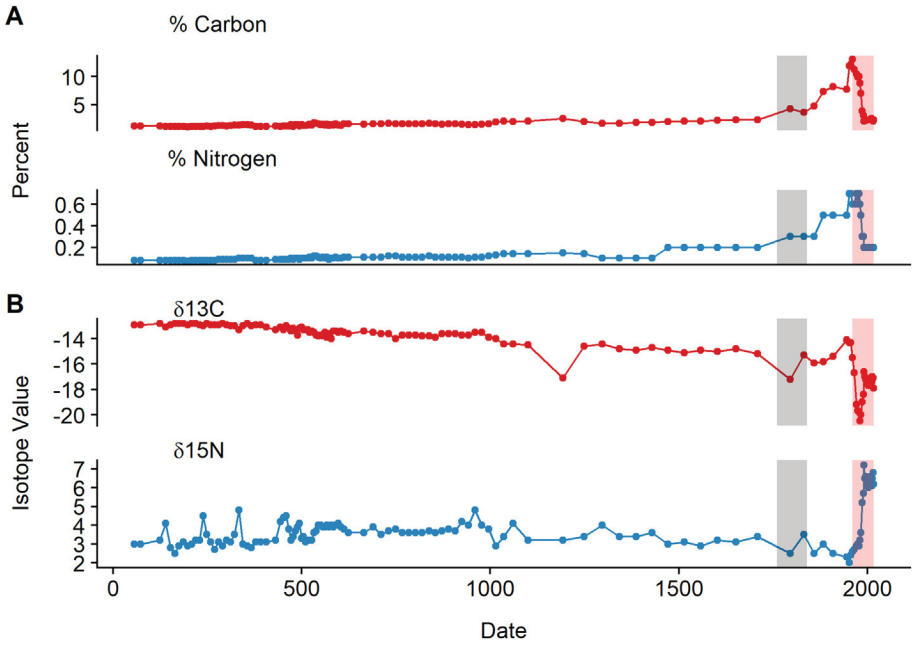

Fig. 9. (A) Percent of carbon (C) and nitrogen (N) and (B) $\delta^{13}C$ and $\delta^{15}N$ in the Upper Wetland core (UC11) from 0 CE to present day. Gray box indicates the Industrial Revolution (~1760–1840) and the red box indicates the deforestation in the Mau Forest (~1964–Present) (Baldyga et al., 2008).

portions of our cores rather than attempt to infer high temporal resolution year-to-year changes due to the uncertainty present in our models (Fig. 3). Our age-depth models and sediment accumulation rates are congruent with contemporary increases in suspended sediment concentrations, prior watershed erosion modelling using remote sensing of land use change, historical precipitation regimes, and the historical water level for Lake Victoria.

Mercury concentrations followed a similar pattern as sediment dynamics in the basin. There was an initial modest increase in mercury concentrations after the late 1700s that was likely caused by atmospheric deposition reflecting global increases in industrialization (Driscoll et al., 2007). The more rapid increase in the 1950s and 1960s was likely due to a combination of deforestation and artisanal mining (Gamby et al., 2015; Telmer and Veiga, 2009), which was also reflected in the large changes in sediment source and quantity during this time. Mercury binds to organic material and will remain in forested soils, only becoming mobilized when the soils are disturbed through deforestation or other land use conversions (Gamby et al., 2015; Schwesig et al., 1999). Similar increases in mercury concentration were documented in response to loss of native land cover in the Amazon during the same time period (Roulet et al., 2000). However, the decline in the 1980s, stabilizing at concentrations only slightly elevated above the historical baseline, suggests there has been a reduction in mercury loads into the Mara Wetland over the last 20 years (Fig. 8). The recent decrease in mercury concentration could be due to the higher relative impact of initial loss of native land cover that is now stabilizing, or to conservation initiatives in the upper basin aimed at decreasing soil erosion and runoff (Gamby et al., 2015). There are no available data about the historical

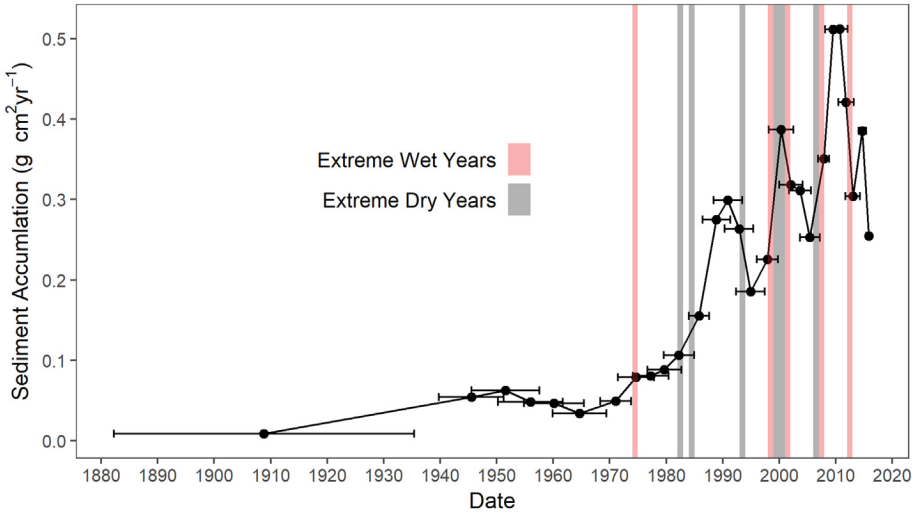

Fig. 10. Sediment accumulation for the Upper Wetland core from 1900 until 2015. Horizontal error bars indicate Bayesian modelled uncertainty from the age-depth model. Years experiencing extreme rainfall with a greater than a 10-year return interval for wet years (red) and dry years (gray) are indicted as shaded bars (Bartzke et al., 2018). Yearly rainfall data only available since 1965.

occurrence or frequency of artisanal gold mining in the Mara River basin, which impedes our quantifying the proportion of mercury contamination that can be attributed to this process.

All mercury concentrations are below the National Oceanic and Atmospheric Administration's (NOAA) Effects Range-Low (150 ppb; ERL) concentration, which was associated with adverse biological effects in 10% of studies reviewed by NOAA, suggesting that current mercury contamination is unlikely to pose an ecological risk in the Mara Wetland. Our data also suggest the wetland may be acting as a sink for mercury contamination in the upper and middle reaches. This region of the wetland is hypoxic due to high decomposition rates of organic material, and mercury in low oxygen environments is transformed into methyl mercury, which is the form most toxic to living organisms (Hong et al., 2012; Sweet and Zelikoff, 2001). However, mercury can bioaccumulate within the food web and be present in toxic levels within piscivorous fish (Driscoll et al., 2007), which can be difficult to estimate from ambient environmental concentrations (Munthe et al., 2007). Because we did not directly measure mercury concentrations in fish, we cannot completely rule out the possibility of harmful levels of mercury within the food web.

Patterns of land use change in the basin are also reflected in increasing concentrations of C and N in wetland sediments over time, likely due to increased organic loading into the river. This pattern is generally mirrored by the C:N ratio, which can indicate the relative degree of aquatic or terrestrial production in the river (Cross et al., 2003; Kaushal and Binford, 1999). Terrestrial production that has entered the river typically has a higher C:N ratio, while aquatic production occurring within the river typically has a lower ratio. Thus, the increase and peak in C:N that occurs from ~1950–1970 and aligns with the increased percent of C and N loading likely indicates an influx of terrestrially-derived production entering the river as a result of deforestation and land cover change (Kaushal and Binford, 1999; Neill et al., 2001) (Figs. 9 and S9).

Both $\delta^{13}C$ and $\delta^{15}N$ were relatively stable over historical time scales from ~2000 years BP until significant anthropogenic change began occurring in the latter half of the 20th century (Fig. 9B). The general trend in the $\delta^{13}C$ of organic carbon to more negative values may indicate increasing tree cover relative to grass cover on the landscape. Trees in this region are predominantly C3 plants with a $\delta^{13}C$ around −28‰, and savanna grasses are predominantly C4 plants with a $\delta^{13}C$ around −14‰ (Masese et al., 2015; Masese et al., 2018). Some of this decline (~2‰) can also be explained by a negative shift in $\delta^{13}C$ due to fossil fuels in the atmosphere (Cerling and Harris, 1999; Francey et al., 1999). More complicated subsequent changes (between 1950 and 1990) could arise from a combination of factors. Significant changes in wildlife populations did occur during this time, and hippos in particular load large amounts of savanna grass into the river during daily feeding migrations (Subalusky et al., 2015). The earliest surveys of hippos in the Mara, conducted in 1959, showed very low numbers that were likely lower than historical abundances (Darling, 1960). Populations then increased exponentially in surveys conducted in 1971 (Olivier and Laurie, 1974) and 1980 (Karstad and Hudson, 1984), and then generally stabilized through 2006 (Kanga et al., 2011). The apparent decrease and subsequent increase in organic C from savanna grasses might thus represent a lagged response to the decline and recovery of hippos. Other factors also may also contribute, including changes in plant community composition in the landscape and in the wetland, changing size of the wetland, and other landscape level patterns including increased burning and deforestation.

Changes in $\delta^{15}N$ indicate an increase in anthropogenic nutrient loading into the river beginning in the 1960s and becoming more significant in the 1980s until stabilizing more recently. Other studies have shown that anthropogenic inputs (via agricultural runoff and sewage) are elevated in nitrogen, and that anthropogenic N is enriched in ^{15}N producing elevated $\delta^{15}N$ compared to non-anthropogenic sources (McClelland et al., 1997).

Changes in erosion processes throughout the basin were likely caused by significant changes in land use and land cover that were coincident with both the eradication of rinderpest and increasing deforestation in the basin. Rinderpest was first found in the Mara region in the 1890s (Percival, 1985) and decimated populations of wild and domestic animals; however, it had been virtually eradicated by 1963 (Talbot and Talbot, 1963), likely due to the vaccination campaign of domestic animals by the local governments (Mariner et al., 2012) and the development of a natural immunity by wildebeest (Plowright and McCulloch, 1967; Sinclair, 1979; Taylor and Watson, 1967). The corresponding increase in livestock and wildlife in the mid-1960s also coincided with the beginning of legal and illegal settlements in the Mau Forest (Baldyga et al., 2008).

5. Conclusions

The Mara Wetland is influenced by changes in the Mara River basin and likely plays an important role in mitigating how those changes influence Lake Victoria. The wetland acts as a sediment trap, with sediment accumulating at higher rates in the Upper Wetland than the Lower Wetland. This wetland function has likely reduced the impact on Lake Victoria of increased sediment transport from the basin since the mid-1900s. Sediment deposition may have contributed to an increase in the size of the Mara Wetland that was proposed to have occurred in the mid-1900s (Mati et al., 2008). The Mara Wetland also appears to act as a sink for mercury contamination, as a large peak in mercury concentration in the Upper Wetland has yet to emerge in the Middle or Lower Wetland sites. Although retention of mercury in the wetland may positively impact the mercury concentrations reaching Lake Victoria, it does raise conservation and health concerns due to the potential transformation of mercury into methyl mercury, which is the form most toxic to people and animals (Hong et al., 2012).

We also observed that downstream effects of landcover and land use change can be significant and can be exacerbated by changing precipitation patterns (Nearing et al., 2005). Increasing extreme rainfall events have likely exacerbated the already increasing sedimentation rates within the basin (Mango et al., 2011). Throughout East Africa, sedimentation has likely increased and will continue to increase as the region continues to receive a higher frequency of extreme rainfall events (Bartzke et al., 2018; Muthoni et al., 2018). Basin-wide historical changes we observed in the Mara Wetland cores are likely indicative of changes occurring throughout the region (Guzha et al., 2018) and provide a historical context to the consequences of increasing development coupled with increasing rainfall variability. Combining age-depth modelling with sediment fingerprinting can help reconstruct historical sedimentation patterns in the context of land use changes in understudied regions.

Acknowledgements

We thank the Republic of Kenya, the United Republic of Tanzania, Andrew McVey and WWF for helping initiate this research. We also thank the Musoma office of the Tanzanian Fisheries Surveillance Office for providing boats and assistance in the field. Mwasiti Rashid, Renata Montserrat, and Ella Jourdain provided assistance in the field and laboratory.

Funding

This work was supported by WWF-UK, WWF-Tanzania and WWF-Kenya Program Offices. Funding was also provided by grants from the National Science Foundation to DMP (DEB 1354053 and 1753727) and EJR (DEB 1354062). The findings and conclusions in this article are those of the authors and do not necessarily represent the views of the U.S. National Park Service.

Appendix A. Supplementary data

Supplementary data to this article can be found online at https://doi.org/10.1016/j.scitotenv.2019.01.421.

References

Abril, J.M., San Miguel, E.G., Ruiz-Canovas, C., Casas-Ruiz, M., Bolívar, J.P., 2018. From floodplain to aquatic sediments: radiogeochronological fingerprints in a sediment core from the mining impacted Sancho Reservoir (SW Spain). Sci. Total Environ. 631-632, 866–878. https://doi.org/10.1016/j.scitotenv.2018.03.114.

Aquino-López, M.A., Blaauw, M., Christen, J.A., Sanderson, N.K., 2018. Bayesian analysis of 210Pb dating. J. Agric. Biol. Environ. Stat. 23, 317–333. https://doi.org/10.1007/s13253-018-0328-7.

Århem, K., Fredén, F., 2014. Land Cover Change and Its Influence on Soil Erosion in the Mara Region, Tanzania: Using Satellite Remote Sensing and the Revised Universal Soil Loss Equation (RUSLE) to Map Land Degradation Between 1986 and 2013. (Student thesis series). INES.

Arias-Ortiz, A., Masqué, P., Garcia-Orellana, J., Serrano, O., Mazarrasa, I., Marbà, N., et al., 2018. Reviews and syntheses: 210Pb-derived sediment and carbon accumulation rates in vegetated coastal ecosystems – setting the record straight. Biogeosciences 15, 6791–6818. https://doi.org/10.5194/bg-15-6791-2018.

Bachmann, W.R., Hoyer, V.M., Canfield, E.D., 2018. Possible sediment mixing and the disparity between field measurements and paleolimnological inferences in shallow Iowa Lakes in the Midwestern United States. Geosciences 8. https://doi.org/10.3390/geosciences8020040.

Baldyga, T.J., Miller, S.N., Driese, K.L., Gichaba, C.M., 2008. Assessing land cover change in Kenya's Mau Forest region using remotely sensed data. Afr. J. Ecol. 46, 46–54. https://doi.org/10.1111/j.1365-2028.2007.00806.x.

Bartzke, G.S., Ogutu, J.O., Mukhopadhyay, S., Mtui, D., Dublin, H.T., Piepho, H.-P., 2018. Rainfall trends and variation in the Maasai Mara ecosystem and their implications for animal population and biodiversity dynamics. PLoS ONE 13, e0202814. https://doi.org/10.1371/journal.pone.0202814.

Baskaran, M., Nix, J., Kuyper, C., Karunakara, N., 2014. Problems with the dating of sediment core using excess 210Pb in a freshwater system impacted by large scale watershed changes. J. Environ. Radioact. 138, 355–363. https://doi.org/10.1016/j.jenvrad.2014.07.006.

Bavor, H.J., Waters, M.T., 2008. Buffering performance in a papyrus-dominated wetland system of the Kenyan portion of the Lake Victoria Basin. In: Vymazal, J. (Ed.), Wastewater Treatment, Plant Dynamics and Management in Constructed and Natural Wetlands. Springer Netherlands, Dordrecht, pp. 33–38 https://doi.org/10.1007/978-1-4020-8235-1_4.

Benoit, G., Rozan, T.F., 2001. 210Pb and 137Cs dating methods in lakes: a retrospective study. J. Paleolimnol. 25, 455–465. https://doi.org/10.1023/A:1011179318352.

Blaauw, M., Christen, J.A., 2011. Flexible paleoclimate age-depth models using an autoregressive gamma process. Bayesian Anal. 6, 457–474. https://doi.org/10.1214/11-BA618.

Blake, W.H., Boeckx, P., Stock, B.C., Smith, H.G., Bodé, S., Upadhayay, H.R., et al., 2018. A deconvolutional Bayesian mixing model approach for river basin sediment source apportionment. Sci. Rep. 8, 13073. https://doi.org/10.1038/s41598-018-30905-9.

Bronk, Ramsey C., 2008. Radiocarbon dating: revolutions in understanding. Archaeometry 50, 249–275. https://doi.org/10.1111/j.1475-4754.2008.00394.x.

Cerling, T.E., Harris, J.M., 1999. Carbon isotope fractionation between diet and bioapatite in ungulate mammals and implications for ecological and paleoecological studies. Oecologia 120, 347–363. https://doi.org/10.1007/s004420050868.

Christen, J.A., Fox, C., 2010. A general purpose sampling algorithm for continuous distributions (the t-walk). Bayesian Anal. 5, 263–281. https://doi.org/10.1214/10-BA603.

Collins, A.L., Pulley, S., Foster, I.D.L., Gellis, A., Porto, P., Horowitz, A.J., 2017. Sediment source fingerprinting as an aid to catchment management: a review of the current state of knowledge and a methodological decision-tree for end-users. J. Environ. Manag. 194, 86–108. https://doi.org/10.1016/j.jenvman.2016.09.075.

Comans, R.N.J., Middelburg, J.J., Zonderhuis, J., Woittiez, J.R.W., Lange, G.J.D., Das, H.A., et al., 1989. Mobilization of radiocaesium in pore water of lake sediments. Nature 339, 367. https://doi.org/10.1038/339367a0.

Cross, W.F., Benstead, J.P., Rosemond, A.D., Bruce, Wallace J., 2003. Consumer-resource stoichiometry in detritus-based streams. Ecol. Lett. 6, 721–732. https://doi.org/10.1046/j.1461-0248.2003.00481.x.

Cutshall, N.H., Larsen, I.L., Olsen, C.R., 1983. Direct analysis of Pb-210 in sediment samples: self-absorption corrections. Nucl. Inst. Methods 206, 309–312.

Darling, F.F., 1960. An ecological reconnaissance of the Mara Plains in Kenya Colony. Wildl. Monogr. 3–41.

Davis, R.B., Hess, C.T., Norton, S.A., Hanson, D.W., Hoagland, K.D., Anderson, D.S., 1984. 137Cs and 210Pb dating of sediments from soft-water lakes in New England (USA) and Scandinavia, a failure of 137Cs dating. Chem. Geol. 44, 151–185. https://doi.org/10.1016/0009-2541(84)90071-8.

Defersha, M.B., Melesse, A.M., McClain, M.E., 2012. Watershed scale application of WEPP and EROSION 3D models for assessment of potential sediment source areas and runoff flux in the Mara River Basin, Kenya. Catena 95, 63–72. https://doi.org/10.1016/j.catena.2012.03.004.

Drexler, J.Z., Fuller, C.C., Archfield, S., 2018. The approaching obsolescence of 137Cs dating of wetland soils in North America. Quat. Sci. Rev. 199, 83–96. https://doi.org/10.1016/j.quascirev.2018.08.028.

Driscoll, C.T., Han, Y.-J., Chen, C.Y., Evers, D.C., Lambert, K.F., Holsen, T.M., et al., 2007. Mercury contamination in forest and freshwater ecosystems in the northeastern United States. Bioscience 57, 12.

Dutton, C., Anisfeld, S., Ernstberger, H., 2013. A novel sediment fingerprinting method using filtration: application to the Mara River, East Africa. J. Soils Sediments 13, 1708–1723. https://doi.org/10.1007/s11368-013-0725-z.

Dutton, C.L., Subalusky, A.L., Anisfeld, S.C., Njoroge, L., Rosi, E.J., Post, D.M., 2018. The influence of a semi-arid sub-catchment on suspended sediments in the Mara River, Kenya. PLoS ONE 13, e0192828. https://doi.org/10.1371/journal.pone.0192828.

Dutton, C.L., Subalusky, A.L., Hill, T.D., Aleman, J.C., Rosi, E.J., Onyango, K.B., et al., 2019. Data for: a 2000-year sediment record reveals rapidly changing sedimentation and land use since the 1960s in the Upper Mara-Serengeti Ecosystem. Mendeley Data. v1 https://doi.org/10.17632/vfd5vzm6rm.1.

FAO, 2018. FAOSTAT Statistics Database. FAO.

Foley, J.A., DeFries, R., Asner, G.P., Barford, C., Bonan, G., Carpenter, S.R., et al., 2005. Global consequences of land use. Science 309, 570–574. https://doi.org/10.1126/science.1111772.

Francey, R.J., Allison, C.E., Etheridge, D.M., Trudinger, C.M., Enting, I.G., Leuenberger, M., et al., 1999. A 1000-year high precision record of δ13C in atmospheric CO_2. Tellus B 51, 170–193. https://doi.org/10.1034/j.1600-0889.1999.t01-1-00005.x.

Gamby, R.L., Hammerschmidt, C.R., Costello, D.M., Lamborg, C.H., Runkle, J.R., 2015. Deforestation and cultivation mobilize mercury from topsoil. Sci. Total Environ. 532, 467–473. https://doi.org/10.1016/j.scitotenv.2015.06.025.

Guzha, A.C., Rufino, M.C., Okoth, S., Jacobs, S., Nóbrega, R.L.B., 2018. Impacts of land use and land cover change on surface runoff, discharge and low flows: evidence from East Africa. J. Hydrol. 15, 49–67. https://doi.org/10.1016/j.ejrh.2017.11.005.

Haslett, J., Parnell, A., 2008. A simple monotone process with application to radiocarbon-dated depth chronologies. J. R. Stat. Soc.: Ser. C: Appl. Stat. 57, 399–418. https://doi.org/10.1111/j.1467-9876.2008.00623.x.

Hoffman, C.M., 2007. Geospatial Mapping and Analysis of Water Availability-demand-use Within the Mara River Basin. (Msc). Florida International University, Miami.

Holdo, R.M., Holt, R.D., Fryxell, J.M., 2009. Opposing rainfall and plant nutritional gradients best explain the wildebeest migration in the Serengeti. Am. Nat. 173, 431–445. https://doi.org/10.1086/597229.

Hong, Y.-S., Kim, Y.-M., Lee, K.-E., 2012. Methylmercury exposure and health effects. J. Prev. Med. Public Health 45, 353–363. https://doi.org/10.3961/jpmph.2012.45.6.353.

Hopcraft, J.G.C., Sinclair, A.R.E., Holdo, R.M., Mwangomo, E., Mduma, S., Thirgood, S., et al., 2013. Why are wildebeest the most abundant herbivore in the Serengeti ecosystem? Serengeti IV: Sustaining Biodiversity in a Coupled Human–natural System. University of Chicago Press, Chicago, Illinois, USA

Jaschinski, S., Hansen, T., Sommer, U., 2008. Effects of acidification in multiple stable isotope analyses. Limnol. Oceanogr. Methods 6, 12–15. https://doi.org/10.4319/lom.2008.6.12.

Kanga, E.M., Ogutu, J.O., Olff, H., Santema, P., 2011. Population trend and distribution of the vulnerable common hippopotamus *Hippopotamus amphibius* in the Mara Region of Kenya. Oryx 45, 20–27.

Kansiime, F., Saunders, M.J., Loiselle, S.A., 2007. Functioning and dynamics of wetland vegetation of Lake Victoria: an overview. Wetl. Ecol. Manag. 15, 443–451. https://doi.org/10.1007/s11273-007-9043-9.

Karstad, E.L., Hudson, R.J., 1984. Census of the Mara River hippopotamus (Hippopotamus amphibius), southwest Kenya, 1980–1982. Afr. J. Ecol. 22, 143–147. https://doi.org/10.1111/j.1365-2028.1984.tb00687.x.

Kassenga, G.R., 1997. A descriptive assessment of the wetlands of the Lake Victoria basin in Tanzania. Resour. Conserv. Recycl. 20, 127–141. https://doi.org/10.1016/S0921-3449(97)00014-1.

Kaushal, S., Binford, M.W., 1999. Relationship between C:N ratios of lake sediments, organic matter sources, and historical deforestation in Lake Pleasant, Massachusetts, USA. J. Paleolimnol. 22, 439–442. https://doi.org/10.1023/a:1008027028029.

Kemp, A.C., Horton, B.P., Vane, C.H., Bernhardt, C.E., Corbett, D.R., Engelhart, S.E., et al., 2013. Sea-level change during the last 2500 years in New Jersey, USA. Quat. Sci. Rev. 81, 90–104. https://doi.org/10.1016/j.quascirev.2013.09.024.

Kirchner, G., 2011. 210Pb as a tool for establishing sediment chronologies: examples of potentials and limitations of conventional dating models. J. Environ. Radioact. 102, 490–494. https://doi.org/10.1016/j.jenvrad.2010.11.010.

Kruskal, W.H., Wallis, W.A., 1952. Use of ranks in one-criterion variance analysis. J. Am. Stat. Assoc. 47, 583–621. https://doi.org/10.1080/01621459.1952.10483441.

Kundzewicz, Z.W., 1997. Water resources for sustainable development. Hydrol. Sci. J. 42, 467–480. https://doi.org/10.1080/02626669709492047.

LVBC, WWF-ESARPO, 2010. Assessing Reserve Flows for the Mara River, Kenya and Tanzania. Lake Victoria Basin Commission of the East African Community, Kisumu.

Mabit, L., Benmansour, M., Abril, J.M., Walling, D.E., Meusburger, K., Iurian, A.R., et al., 2014. Fallout 210Pb as a soil and sediment tracer in catchment sediment budget investigations: a review. Earth Sci. Rev. 138, 335–351. https://doi.org/10.1016/j.earscirev.2014.06.007.

Mango, L.M., Melesse, A.M., McClain, M.E., Gann, D., Setegn, S.G., 2011. Land use and climate change impacts on the hydrology of the upper Mara River Basin, Kenya: results of a modeling study to support better resource management. Hydrol. Earth Syst. Sci. 15, 2245–2258.

Mariner, J.C., House JA, Mebus, C.A., Sollod, A.E., Chibeu, D., Jones, B.A., et al., 2012. Rinderpest eradication: appropriate technology and social innovations. Science 337, 1309–1312. https://doi.org/10.1126/science.1223805.

Masese, F.O., Abrantes, K.G., Gettel, G.M., Bouillon, S., Irvine, K., McClain, M.E., 2015. Are large herbivores vectors of terrestrial subsidies for riverine food webs? Ecosystems 18, 686–706. https://doi.org/10.1007/s10021-015-9859-8.

Masese, F.O., Abrantes, K.G., Gettel, G.M., Irvine, K., Bouillon, S., McClain, M.E., 2018. Trophic structure of an African savanna river and organic matter inputs by large

terrestrial herbivores: a stable isotope approach. Freshw. Biol. https://doi.org/10.1111/fwb.13163.
Mati, B.M., Mutie, S., Gadain, H., Home, P., Mtalo, F., 2008. Impacts of land-use/cover changes on the hydrology of the transboundary Mara River, Kenya/Tanzania. Lakes Reserv. Res. Manag. 13, 169–177. https://doi.org/10.1111/j.1440-1770.2008.00367.x.
Mayo, A.W., Muraza, M., Norbert, J., 2013. The role of Mara River Basin Wetland in reduction of nitrogen load to Lake Victoria. Int. J. Water Resour. Environ. Eng. 5, 659–669. https://doi.org/10.5897/IJWREE2013.0444.
McClain, M.E., 2013. Balancing water resources development and environmental sustainability in Africa: a review of recent research findings and applications. Ambio 42, 549–565. https://doi.org/10.1007/s13280-012-0359-1.
McClain, M.E., Subalusky, A.L., Anderson, E.P., Dessu, S.B., Melesse, A.M., Ndomba, P.M., et al., 2014. Comparing flow regime, channel hydraulics, and biological communities to infer flow–ecology relationships in the Mara River of Kenya and Tanzania. Hydrol. Sci. J. 59, 801–819. https://doi.org/10.1080/02626667.2013.853121.
McClelland, J.W., Valiela, I., Michener, R.H., 1997. Nitrogen-stable isotope signatures in estuarine food webs: a record of increasing urbanization in coastal watersheds. Limnol. Oceanogr. 42, 930–937. https://doi.org/10.4319/lo.1997.42.5.0930.
Mduma, S.A.R., Sinclair, A.R.E., Hilborn, R., 1999. Food regulates the Serengeti wildebeest: a 40-year record. J. Anim. Ecol. 68, 1101–1122. https://doi.org/10.1046/j.1365-2656.1999.00352.x.
Moore, J.W., Semmens, B.X., 2008. Incorporating uncertainty and prior information into stable isotope mixing models. Ecol. Lett. 11, 470–480. https://doi.org/10.1111/j.1461-0248.2008.01163.x.
Munthe, J., Bodaly, R.A., Branfireun, B.A., Driscoll, C.T., Gilmour, C.C., Harris, R., et al., 2007. Recovery of mercury-contaminated fisheries. Ambio 36, 12.
Muthoni, F.K., Odongo, V.O., Ochieng, J., Mugalavai, E.M., Mourice, S.K., Hoesche-Zeledon, I., et al., 2018. Long-term spatial-temporal trends and variability of rainfall over Eastern and Southern Africa. Theor. Appl. Climatol. https://doi.org/10.1007/s00704-018-2712-1.
Mwangi, M.H., Lariu, P., Julich, S., Patil, D.S., McDonald, A.M., Feger, K.-H., 2018. Characterizing the intensity and dynamics of land-use change in the Mara River Basin, East Africa. Forests 9. https://doi.org/10.3390/f9010008.
Nearing, M.A., Jetten, V., Baffaut, C., Cerdan, O., Couturier, A., Hernandez, M., et al., 2005. Modeling response of soil erosion and runoff to changes in precipitation and cover. Catena 61, 131–154. https://doi.org/10.1016/j.catena.2005.03.007.
Neill, C., Deegan, L.A., Thomas, S.M., Cerri, C.C., 2001. Deforestation for pasture alters nitrogen and phosphorus in small Amazonian streams. Ecol. Appl. 11, 1817–1828. https://doi.org/10.2307/3061098.
Nyarko, E., Klubi, E., Laissaoui, A., Benmansour, M., 2016. Estimating recent sedimentation rates using lead-210 in tropical estuarine systems: case study of Volta and Pra estuaries in Ghana, West Africa. J. Oceanogr. Mar. Res. https://doi.org/10.4172/2572-3103.1000141.
Odada, E.O., Olago, D.O., Kulindwa, K., Ntiba, M., Wandiga, S., 2004. Mitigation of environmental problems in Lake Victoria, East Africa: causal chain and policy options analyses. AMBIO J. Hum. Environ. 33, 13–23. https://doi.org/10.1579/0044-7447-33.1.13.
Ogutu, J.O., Owen-Smith, N., Piepho, H.P., Said, M.Y., 2011. Continuing wildlife population declines and range contraction in the Mara region of Kenya during 1977–2009. J. Zool. 285, 99–109. https://doi.org/10.1111/j.1469-7998.2011.00818.x.
Ogutu, J.O., Piepho, H.-P., Said, M.Y., Ojwang, G.O., Njino, L.W., Kifugo, S.C., et al., 2016. Extreme wildlife declines and concurrent increase in livestock numbers in Kenya: what are the causes? PLoS ONE 11, e0163249. https://doi.org/10.1371/journal.pone.0163249.
Olang, L.O., Kundu, P.M., 2011. Land degradation of the Mau forest complex in Eastern Africa: a review for management and restoration planning. Environmental Monitoring. InTech.
Oldfield, F., Appleby, P.G., 1984. Empirical testing of 210Pb-dating models for lake sediments. In: Haworth, E.Y., Lund, J.W.G. (Eds.), Lake Sediments and Environmental History. University of Minnesota, Minneapolis, MN, pp. 93–124.
Olivier, R.C.D., Laurie, W.A., 1974. Habitat utilization by hippopotamus in the Mara River*. Afr. J. Ecol. 12, 249–271. https://doi.org/10.1111/j.1365-2028.1974.tb01036.x.
O'Sullivan, J.J., Lupakisyo Mwalwiba, G., Purcell, P.J., Turner, J.N., Mtalo, F., 2016. Assessing sediment and water quality issues in expanding African wetlands: the case of the Mara River, Tanzania. Int. J. Environ. Stud. 73, 95–107. https://doi.org/10.1080/00207233.2015.1116226.
Parnell, A.C., 2016. Bchron: Radiocarbon Dating, Age-depth Modelling, Relative Sea Level Rate Estimation, and Non-parametric Phase Modelling.
Percival, A.B., 1985. A Game Ranger on Safari. Amwell Press, Clinton, N.J.
Plowright, W., McCulloch, B., 1967. Investigations on the incidence of rinderpest virus infection in game animals of N. Tanganyika and S. Kenya 1960/63. Epidemiol. Infect. 65, 343–358.
R Core Team, 2018. R: A Language and Environment for Statistical Computing. R Foundation for Statistical Computing, Vienna, Austria.
Raikes, P.L., 1981. Livestock Development and Policy in East Africa. Nordic Africa Institute.
Ramnarine, R., Voroney, R.P., Wagner-Riddle, C., Dunfield, K.E., 2011. Carbonate removal by acid fumigation for measuring the δ13C of soil organic carbon. Can. J. Soil Sci. 91, 247–250. https://doi.org/10.4141/cjss10066.
Reimer, P.J., Bard, E., Bayliss, A., Beck, J.W., Blackwell, P.G., Ramsey, C.B., et al., 2013. IntCal13 and Marine13 radiocarbon age calibration curves 0–50,000 years cal BP. Radiocarbon 55, 1869–1887. https://doi.org/10.2458/azu_js_rc.55.16947.
Ritchie, J.C., McHenry, J.R., 1990. Application of radioactive fallout cesium-137 for measuring soil erosion and sediment accumulation rates and patterns: a review. J. Environ. Qual. 19, 215–233. https://doi.org/10.2134/jeq1990.00472425001900020006x.
Robbins, J.A., 1978. Geochemical and geophysical applications of radioactive lead. In: Nriagu, J.O. (Ed.), Biogeochemistry of Lead in the Environment. Elsevier, pp. 285–393.
Roulet, M., Lucotte, M., Canuel, R., Farella, N., Courcelles, M., Guimarães, J.R.D., et al., 2000. Increase in mercury contamination recorded in lacustrine sediments following deforestation in the central Amazon1The present investigation is part of an ongoing study, the CARUSO project (CRDI-UFPa-UQAM), initiated to determine the sources, fate and health effects of the presence of MeHg in the area of the Lower Tapajós. Chem. Geol. 165, 243–266. https://doi.org/10.1016/S0009-2541(99)00172-2.
RStudio Team, 2016. RStudio: Integrated Development for R. RStudio, Inc., Boston, MA.
Saldarriaga-Isaza, A., Villegas-Palacio, C., Arango, S., 2015. Phasing out mercury through collective action in artisanal gold mining: evidence from a framed field experiment. Ecol. Econ. 120, 406–415. https://doi.org/10.1016/j.ecolecon.2015.04.004.
Scheren, P.A.G.M., Zanting, H.A., Lemmens, A.M.C., 2000. Estimation of water pollution sources in Lake Victoria, East Africa: application and elaboration of the rapid assessment methodology. J. Environ. Manag. 58, 235–248. https://doi.org/10.1006/jema.2000.0322.
Schwesig, D., Ilgen, G., Matzner, E., 1999. Mercury and methylmercury in upland and wetland acid forest soils of a watershed in NE-Bavaria, Germany. Water Air Soil Pollut. 113, 141–154.
Sharma, N.P., Damhaug, T., Gilgan-Hunt, E., Grey, D., Okaru, V., Rothberg, D., 1996. African Water Resources; Challenges and Opportunities for Sustainable Development.
Shillington, K., 2012. History of Africa. Palgrave Macmillan, London; New York, NY.
Sinclair, A., 1979. The eruption of the ruminants. Serengeti: Dynamics of an Ecosystem, pp. 82–103.
Smith, J.N., 2001. Why should we believe 210Pb sediment geochronologies? J. Environ. Radioact. 55, 121–123. https://doi.org/10.1016/S0265-931X(00)00152-1.
Stock, B.C., Semmens, B.X., 2016. MixSIAR GUI User Manual.
Stock, B.C., Jackson, A.L., Ward, E.J., Parnell, A.C., Phillips, D.L., Semmens, B.X., 2018. Analyzing mixing systems using a new generation of Bayesian tracer mixing models. PeerJ 6, e5096. https://doi.org/10.7717/peerj.5096.
Subalusky, A.L., Dutton, C.L., Rosi-Marshall, E.J., Post, D.M., 2015. The hippopotamus conveyor belt: vectors of carbon and nutrients from terrestrial grasslands to aquatic systems in sub-Saharan Africa. Freshw. Biol. 60. https://doi.org/10.1111/fwb.12474.
Subalusky, A.L., Dutton, C.L., Rosi, E.J., Post, D.M., 2017. Annual mass drownings of the Serengeti wildebeest migration influence nutrient cycling and storage in the Mara River. Proc. Natl. Acad. Sci. 114, 7647–7652. https://doi.org/10.1073/pnas.1614778114.
Sweet, L.I., Zelikoff, J.T., 2001. Toxicology and immunotoxicology of mercury: a comparative review in fish and humans. J. Toxicol. Environ. Health Part B 4, 161–205. https://doi.org/10.1080/10937400117236.
Talbot, L.M., Talbot, M.H., 1963. The wildebeest in Western Masailand, East Africa. Wildl. Monogr. 3–88.
Taylor, W., Watson, R.M., 1967. Studies on the epizootiology of rinderpest in blue wildebeest and other game species of Northern Tanzania and Southern Kenya, 1965–7. Epidemiol. Infect. 65, 537–545.
Telmer, K.H., Veiga, M.M., 2009. World emissions of mercury from artisanal and small scale gold mining. In: Mason, R., Pirrone, N. (Eds.), Mercury Fate and Transport in the Global Atmosphere: Emissions, Measurements and Models. Springer US, Boston, MA, pp. 131–172 https://doi.org/10.1007/978-0-387-93958-2_6.
Turekian, K.K., Benninger, L.K., Dion, E.P., 1983. 7Be and 210Pb total deposition fluxes at New Haven, Connecticut and at Bermuda. J. Geophys. Res. Oceans 88, 5411–5415. https://doi.org/10.1029/JC088iC09p05411.
UN-Water A, 2003. The Africa Water Vision for 2025: Equitable and Sustainable Use of Water for Socioeconomic Development.
Vanderkelen, I., van Lipzig, N.P.M., Thiery, W., 2018. Modelling the water balance of Lake Victoria (East Africa) – part 1: observational analysis. Hydrol. Earth Syst. Sci. 22, 5509–5525. https://doi.org/10.5194/hess-22-5509-2018.
Venables, W.N., Ripley, B.D., 2002. Modern Applied Statistics With S. Springer, New York https://doi.org/10.1007/978-0-387-21706-2.
Vörösmarty, C.J., Green, P., Salisbury, J., Lammers, R.B., 2000. Global water resources: vulnerability from climate change and population growth. Science 289, 284–288. https://doi.org/10.1126/science.289.5477.284.
Wallbrink, P.J., Murray, A.S., Olley, J.M., Olive, L.J., 1998. Determining sources and transit times of suspended sediment in the Murrumbidgee River, New South Wales, Australia, using fallout 137Cs and 210Pb. Water Resour. Res. 34, 879–887. https://doi.org/10.1029/97WR03471.
Walling, D.E., Owens, P.N., Carter, J., Leeks, G.J.L., Lewis, S., Meharg, A.A., et al., 2003. Storage of sediment-associated nutrients and contaminants in river channel and floodplain systems. Appl. Geochem. 18, 195–220. https://doi.org/10.1016/S0883-2927(02)00121-X.
Wang, J., Baskaran, M., Niedermiller, J., 2017. Mobility of 137Cs in freshwater lakes: a mass balance and diffusion study of Lake St. Clair, Southeast Michigan, USA. Geochim. Cosmochim. Acta 218, 323–342. https://doi.org/10.1016/j.gca.2017.09.017.
Weihs, C., Ligges, U., Luebke, K., Raabe, N., 2005. klaR analyzing German business cycles. In: Baier, D., Decker, R., Schmidt-Thieme, L. (Eds.), Data Analysis and Decision Support. Springer-Verlag, Berlin, pp. 335–343 https://doi.org/10.1007/3-540-28397-8_36.